Discovery of peptide ligands through docking and virtual screening at nicotinic acetylcholine receptor homology models

Abba E. Leffler[a], Alexander Kuryatov[b], Henry A. Zebroski[c], Susan R. Powell[c], Petr Filipenko[d,e,f], Adel K. Hussein[g,h], Juliette Gorson[d,e,f,h], Anna Heizmann[i], Sergey Lyskov[j], Richard W. Tsien[k,1], Sébastien F. Poget[g,h], Annette Nicke[i], Jon Lindstrom[b], Bernardo Rudy[k], Richard Bonneau[l,m,n], and Mandë Holford[d,e,f,h,1]

[a]Neuroscience Graduate Program, Sackler Institute of Graduate Biomedical Sciences, New York University School of Medicine, New York, NY 10016; [b]Department of Neuroscience, University of Pennsylvania Perelman School of Medicine, Philadelphia, PA 19104; [c]Proteomics Resource Center, The Rockefeller University, New York, NY 10065; [d]Department of Chemistry, Belfer Research Center–Hunter College, New York, NY 10021; [e]Division of Invertebrate Zoology, The American Museum of Natural History, New York, NY 10024; [f]Department of Biochemistry, Weill Cornell Medical College, Cornell University, New York, NY 10021; [g]Department of Chemistry, College of Staten Island, Staten Island, NY 10314; [h]Program in Biochemistry, The Graduate Center, City University of New York, New York, NY 10016; [i]Walther Straub Institute of Pharmacology and Toxicology, LMU Munich, 80336 Munich, Germany; [j]Department of Chemical and Biomolecular Engineering, Johns Hopkins University, Baltimore, MD 21218; [k]NYU Neuroscience Institute and the Department of Neuroscience and Physiology, New York University School of Medicine, New York, NY 10016; [l]Department of Biology, New York University, New York, NY 10003; [m]Courant Institute of Mathematical Sciences, New York University, New York, NY 10012; and [n]Center for Computational Biology, Simons Foundation, New York, NY 10010

Contributed by Richard W. Tsien, August 14, 2017 (sent for review March 9, 2017; reviewed by David J. Adams and Ryan Hibbs)

Venom peptide toxins such as conotoxins play a critical role in the characterization of nicotinic acetylcholine receptor (nAChR) structure and function and have potential as nervous system therapeutics as well. However, the lack of solved structures of conotoxins bound to nAChRs and the large size of these peptides are barriers to their computational docking and design. We addressed these challenges in the context of the α4β2 nAChR, a widespread ligand-gated ion channel in the brain and a target for nicotine addiction therapy, and the 19-residue conotoxin α-GID that antagonizes it. We developed a docking algorithm, ToxDock, which used ensemble-docking and extensive conformational sampling to dock α-GID and its analogs to an α4β2 nAChR homology model. Experimental testing demonstrated that a virtual screen with ToxDock correctly identified three bioactive α-GID mutants (α-GID[A10V], α-GID[V13I], and α-GID[V13Y]) and one inactive variant (α-GID[A10Q]). Two mutants, α-GID[A10V] and α-GID[V13Y], had substantially reduced potency at the human α7 nAChR relative to α-GID, a desirable feature for α-GID analogs. The general usefulness of the docking algorithm was highlighted by redocking of peptide toxins to two ion channels and a binding protein in which the peptide toxins successfully reverted back to near-native crystallographic poses after being perturbed. Our results demonstrate that ToxDock can overcome two fundamental challenges of docking large toxin peptides to ion channel homology models, as exemplified by the α-GID:α4β2 nAChR complex, and is extendable to other toxin peptides and ion channels. ToxDock is freely available at rosie.rosettacommons.org/tox_dock.

homology model | nicotinic receptor | conotoxin | docking | virtual screening

Venom peptide toxins isolated from predatory marine cone snails (conotoxins) are prized research tools due to their native potency and selectivity for ion channels (1–4). Conotoxins have played an especially important role in elucidating how the many different subtypes of the nicotinic acetylcholine receptor (nAChR), a prototypical ligand-gated ion channel, contribute to diseases like nicotine addiction, Parkinson's disease, and neuropathic pain (5–8). Peptide engineering approaches such as alanine scanning and structure-guided mutagenesis have also been remarkably successful at expanding the limits of conotoxin pharmacology to include those nAChRs not naturally targeted by conotoxins (7). However, some promising conotoxins remain challenging to optimize, and some important nAChRs are difficult to target.

The peptide α-GID was the first conotoxin found to have substantial antagonism at the rat α4β2 nAChR, with its IC_{50} reported as 128–152 nM and 4.8 μM (9–11). The α4β2 nAChR is one of the most widely expressed nAChRs in the brain and is a validated target for smoking cessation therapeutics (11–13). The receptor is formed from five homologous subunits, consisting of either two α4 subunits and three β2 subunits or three α4 subunits and two β2 subunits, organized like barrel staves to form a central channel (14). Cations flow through the channel when acetylcholine (ACh) is bound at specific interfaces between subunits in the extracellular domain (14), where α-GID presumably binds competitively (9, 15). In addition to the α4β2 nAChR, α-GID potently antagonizes the rat α3β2 nAChR (IC_{50} reported as 3.1–3.4 nM and 36 nM) as well as the rat α7 nAChR (IC_{50} = 4.5–5.1 nM) (9–11). Consequently, there has been significant interest in engineering an analog of α-GID that antagonizes the α4β2 nAChR but not the α3β2 and α7 nAChRs, especially for the human nAChRs (9–11, 15). A recent study by Banerjee et al. (9) used structure-guided mutagenesis to discover

Significance

Predicting how conotoxins bind to nicotinic acetylcholine receptors (nAChRs) is hard. Not only are these venom-derived peptides large, but the structures of many nAChRs are unknown. In response, we developed an ensemble-docking algorithm named ToxDock. We used ToxDock to reliably dock the conotoxin α-GID to a homology model of the α4β2 nAChR, a main nAChR in the brain and target for nicotine addiction therapeutics. A virtual screen with ToxDock identified four α-GID analogs and, based on experimental evidence, correctly predicted their activity at the α4β2 nAChR in all cases. More screening showed that two of these analogs have substantially reduced antagonism at the human α7 nAChR, a key step in optimizing α-GID into a tool for studying brain nAChRs.

Author contributions: A.E.L., R.W.T., B.R., R.B., and M.H. designed research; A.E.L., A.K., P.F., A.K.H., J.G., A.H., S.L., and S.F.P. performed research; H.A.Z., S.R.P., A.N., and J.L. contributed new reagents/analytic tools; A.E.L., A.K., R.W.T., S.F.P., A.N., J.L., B.R., R.B., and M.H. analyzed data; and A.E.L., R.W.T., B.R., and M.H. wrote the paper.

Reviewers: D.J.A., Illawarra Health and Medical Research Institute; and R.H., University of Texas Southwestern Medical Center.

The authors declare no conflict of interest.

Data deposition: Atomic coordinates and NMR parameters have been deposited in the Protein Data Bank, www.pdb.org (PDB ID codes 5UG3 and 5UG5).

[1]To whom correspondence may be addressed. Email: richard.tsien@nyumc.org or mholford@hunter.cuny.edu.

This article contains supporting information online at www.pnas.org/lookup/suppl/doi:10.1073/pnas.1703952114/-/DCSupplemental.

that α-GID[V18N] is selective for the rat α4β2 nAChR vs. the rat α3β2 nAChR. Developing an α-GID analog that retains its activity at the α4β2 nAChR while having reduced potency at the α7 nAChR has proven difficult. Millard et al. (10) made significant progress in this respect by performing alanine scanning on α-GID to elucidate the structural determinants of its activity at the α4β2 nAChR. They found that five alanine mutants of α-GID retained bioactivity at the α4β2 nAChR, but all also remained potent antagonists of the α7 nAChR (10). Given that the α4β2 and α7 nAChRs are the most abundant nAChRs in the human brain (12, 16), developing an α-GID analog that distinguishes between these two receptors has been, and remains, an important goal.

Docking has emerged as a very useful approach for rationalizing mutagenesis data on conotoxin and nAChR interactions (17–21). Less well understood is whether docking and computational methods can be used to virtually screen for conotoxins with optimized properties, such as potency and selectivity, although recent efforts suggest this may be possible (22, 23). There are two main challenges when docking and virtually screening conotoxins against nAChRs. First, the presence of highly mobile elements in peptide toxins, like the four-residue N-terminal "tail" of α-GID (11), can impact the results of docking simulations (24). Second, although cocrystal structures of conotoxins and a homopentameric soluble surrogate of the nAChR ligand-binding domain [Acetylcholine Binding Protein (AChBP)] have been solved (25), no crystal structure of a conotoxin and nAChR has been reported to date. This is problematic for a virtual screening campaign that uses a homology model of a heteromeric nAChR built on a homomeric AChBP template structure with less than 30% sequence identity to the nAChR, because effective virtual screening requires that the shape of the ligand-bound complex be known to high precision (26, 27). Hypothetically, broad sampling of many different conformational states of both the conotoxin and nAChR homology model could overcome these two issues.

To address these dual challenges, we have developed a docking algorithm, ToxDock, in the context of the conotoxin α-GID and the α4β2 nAChR. ToxDock employs extensive conformational sampling of both the nAChR homology model and the conotoxin peptide to refine models of these complexes by combining two existing protocols in the Rosetta macromolecular modeling suite (28), Rosetta FastRelax and Rosetta FlexPepDock (29, 30) (Fig. 1). In the first stage of ToxDock, the entire complex is relaxed into lower energy states, followed by flexible docking of the conotoxin with ensemble docking in the second step (Fig. 1). In this manner, ToxDock is a refinement algorithm that can simulate a peptide toxin bound to an ion channel, given sufficient data for the bound complex. Using ToxDock, we investigate two principal questions. Can an algorithm that accounts for the conformational flexibility of a toxin peptide:ion channel complex be used to dock α-GID and its analogs to the α4β2 nAChR with confidence? If so, can it also be used to discover new α-GID derivatives bioactive at the α4β2 nAChR, and do any of these new derivatives have novel properties such as reduced potency at the human α7 nAChR?

We undertook both benchmark and prospective docking screens of α-GID analogs against a homology model of the α4β2 nAChR using ToxDock, followed by experimental assays at nAChR subtypes and structural characterization of α-GID analogs. We also sought to obtain additional corroboration of our binding pose for α-GID by docking it into the recently crystallized structure of the α4β2 nAChR in complex with nicotine (31). Docking α-GID to this crystal structure could help confirm the binding mode of α-GID, but studies have also shown that the binding pocket adopts distinctive interfaces depending on whether an agonist or antagonist is present (32–35). Finally, we performed redocking experiments on crystal structures of peptide toxins with two different ion channels and a binding protein to probe the generality of ToxDock. Our extensively benchmarked docking algorithm can overcome some of the fundamental limitations in docking the conotoxin α-GID to the α4β2 nAChR, and may prove useful for other toxin peptide:ion channel systems.

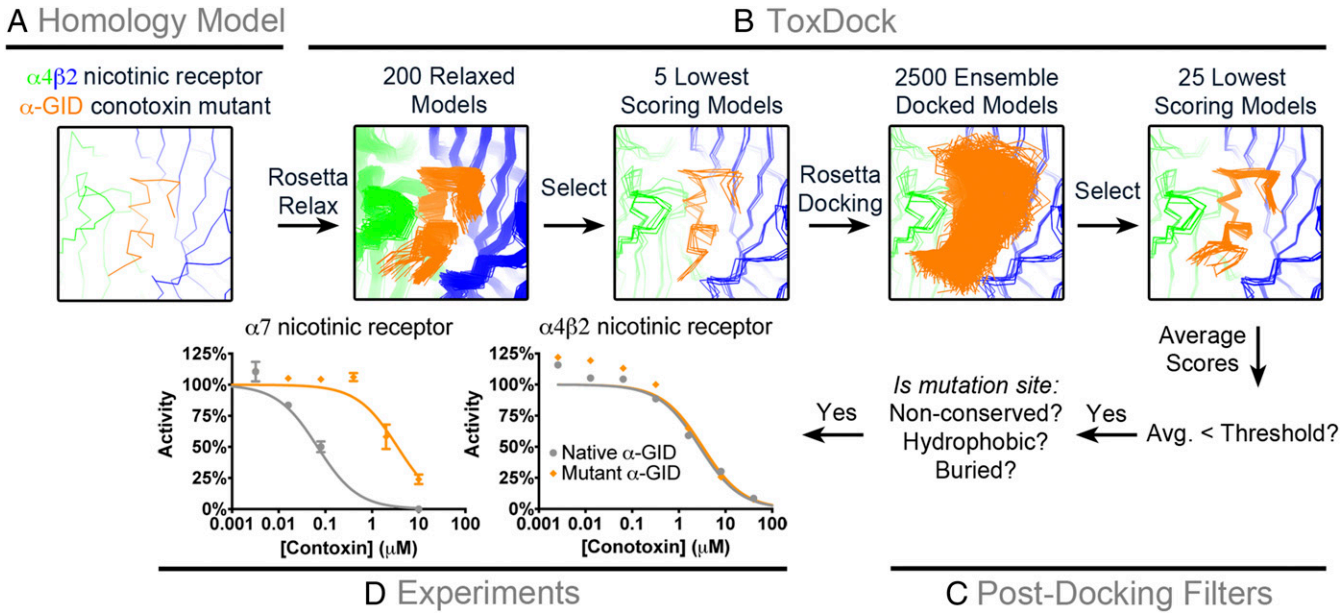

Fig. 1. Overview. (*A*) Initial homology model of an α-GID conotoxin point mutant (orange) in complex with the extracellular domain of the α4β2 nAChR (α4 subunit in green and β2 subunit in blue) is shown. (*B*) Each box shows the models of the complex considered at each step in the ToxDock protocol. Individual models are shown in ribbon representation and aligned. (*C*) Suitability of the conotoxin mutant for synthesis is further assessed by its average (ensemble) docking score to the receptor and the position of its point mutation. (*D*) Abilities of both the native (gray) and orange (mutant) conotoxins to block the responses of nicotinic receptor subtypes to ACh are assessed using fluorescent membrane potential assays. Avg., average.

Results

Development and Benchmarking of ToxDock. Our initial goal was to develop a docking method that could reliably model the α4β2 nAChR in complex with α-GID analogs, without knowing the structure of either. To construct the homology model, five template structures of AChBP from *Aplysia californica* in complex with different α-conotoxins (33, 36–38) were used to build 1,000 homology models of the human α4β2 nAChR extracellular subunit dimer using Modeller-9v11 (*SI Appendix*, Fig. S1*A*). The top model, judged by Modeller's Discrete Optimized Protein Energy score, was selected for docking (*SI Appendix*, Fig. S1*B*). Models of six α-GID analogs that are known antagonists of the rat α4β2 nAChR ("bioactives") and 13 analogs that are not ["inactives" (i.e., IC_{50} is much greater than 1 μM)] were added individually to the homology model (10). All models were based on the NMR structure of α-GID (11), and their initial placement was guided by the cocrystal structure of AChBP and an α-PnIA variant (36). These complexes were then subjected to four levels of progressively greater conformational sampling. Our criterion for the performance of each method on the set of mutants was the area under curve (AUC) computed from a receiver operating characteristic plot (39), which indicates the extent to which models refined by each method could rank the six bioactive α-GID analogs over the 13 inactive ones.

At the lowest level of sampling, only the side chains of the receptor and peptide were repacked with Rosetta, and the resulting complexes were ranked by their Rosetta total scores ("Unrefined Model"). Neither the backbone of the peptide nor the receptor was permitted to move. This led to an AUC of 0.64 ± 0.16, which was not statistically different from the AUC of 0.5 that corresponds to a random ranking (Fig. 2*A*). Next, refining each complex by flexibly docking the α-GID analogs 200 times with Rosetta FlexPepDock and calculating a score over the lowest scoring 25 models ("Docking to Unrefined Model") led to a modest improvement in the AUC to 0.69 ± 0.13, but this effect was not significant (Fig. 2*A*). These findings suggested that a more aggressive conformational search was necessary. To this end, we used the Rosetta Relax protocol to sample 200 conformations of the entire complex in which both backbones and side chains were allowed to move (*SI Appendix*, Fig. S2; scores are approximately normally distributed and have a small SD) and docked the α-GID analogs to the lowest scoring model 500 times with Rosetta FlexPepDock. This scheme ("Docking to 1 Relaxed Model") led to a significant improvement, with the AUC climbing to 0.79 ± 0.12 (Fig. 2*A*). Finally, we examined the effect of ensemble docking by docking the α-GID analogs 500 times with FlexPepDock to each of the five lowest scoring models in the relaxed set (Fig. 1). This technique ("ToxDock"; *SI Appendix*, Table S1) was the most successful overall, with an AUC of 0.86 ± 0.10 that is close to the theoretical maximum of 1.0 (Fig. 2). Importantly, all four of the lowest scoring complexes also contained α-GID analogs that are true bioactives at the α4β2 nAChR (*SI Appendix*, Fig. S3). Given the small sample size of the data, we also compared the scores of the bioactives and inactives using Mann–Whitney and permutation tests to ensure the differences in ToxDock scores between the bioactives and inactives were not due to chance. Both tests revealed that the differences in the scores that ToxDock assigned to the two classes were significant ($P = 0.013$ and $P = 0.007$, respectively). These results demonstrate that extensive conformational sampling can produce faithful models of α-GID analogs in complex with an α4β2 nAChR homology model.

We next compared the lowest scoring ToxDock refined model to the starting (unrefined) homology model. The poses were broadly similar but had some important differences (Fig. 2*B*). Specifically, in the ToxDock model, the N-terminal tail of α-GID was compact and somewhat helical, in accordance with previous speculation that this region, which adopts many conformations in its solution NMR structure, may be more defined when in contact with the α4β2 nAChR (40). In contrast, the tail was more extended in the starting pose. The C-terminal region (residues 15–19) also exhibited structural differences, with the ToxDock refined model perturbed from the starting conformation [2.4-Å Cα root mean square deviation (rmsd)]. In terms of the receptor, the ToxDock and starting models were generally similar, even in highly flexible regions on the β2 subunit. One place this was not true was loop C, which ToxDock pushed slightly outward relative to the starting model (Fig. 2*B*). Taken together, it appears that refinement with ToxDock largely resulted in the poses that are still in the general vicinity of the starting model but contain subtle structural differences that cumulatively result in their improved accuracy.

Virtual Screen and Selection of α-GID Mutants. To examine the accuracy of ToxDock at making new predictions, a library of 256 α-GID point mutants was prepared in silico using PyRosetta and the solution NMR structure of native α-GID (11, 41). Each of the peptides was superimposed onto the α4β2 nAChR homology model used in the benchmarking study, using the α-PnIA[A10L,D14K]:AChBP complex as a guide. These complexes were then refined with ToxDock (Fig. 3*A*). After the initial virtual screen, roughly 25% of the α-GID derivatives were predicted to be bioactive at the human

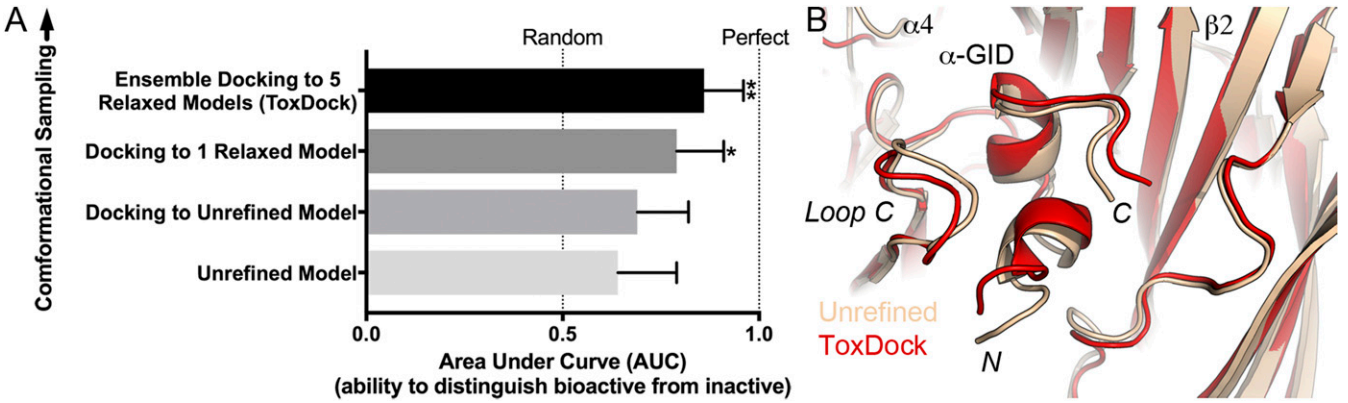

Fig. 2. Benchmarking and validation of ToxDock. (*A*) Performance of different methods on benchmarking the α-GID mutant library. The AUC for each method is plotted as a bar graph, with the error bar indicating the SE of the area under the receiver operating characteristic curve. *$P < 0.05$; **$P \leq 0.01$. Statistical analyses were performed using default settings in GraphPad Prism. (*B*) Comparison of the conformations of the unrefined homology model (wheat) and lowest scoring ToxDock pose (red). All chains of both structures were aligned using PyMOL.

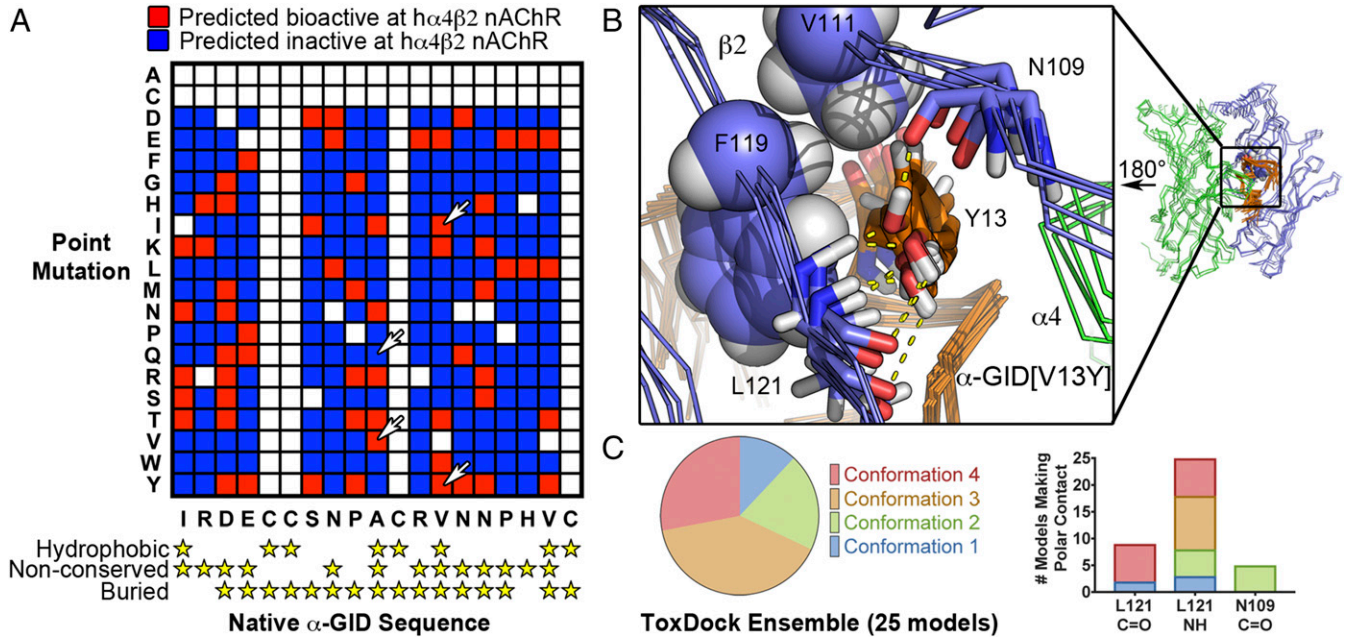

Fig. 3. Virtual screen and predicted binding modes. (*A*) Virtual screen with ToxDock of 256 α-GID point mutants against the α4β2 nAChR homology model. Each square represents an individual ToxDock simulation of a different α-GID point mutant. Red squares are mutants predicted to be bioactive at the human α4β2 nAChR, blue squares are mutants predicted to be inactive, and white squares are mutants that were not simulated. The white arrows point to the four mutants (α-GID[A10V], α-GID[A10Q], α-GID[V13I], and α-GID[V13Y]) chosen for experimental characterization. Gold stars denote positions on α-GID that are nonconserved, hydrophobic, or buried in the α4β2 nAChR homology model. (*B*) Twenty-five lowest scoring ToxDock models ("ToxDock ensemble") of the α4β2 nAChR homology model in complex with α-GID[V13Y] are shown. Side chains are depicted as sticks, with the exception of the V111 and F119 side chains, which are shown as spheres for a single model. The α4 subunit is green, the β2 subunit blue, and the peptide orange. Putative polar contacts are shown as dashed lines. All images were made in PyMOL. (*C*) Statistics of the ToxDock ensemble are shown, such as how many models in each conformation are included in the ToxDock ensemble (pie chart) and the polar contacts formed by each model (stacked bar chart). Numbering of residues is consistent with PDB ID code 5KXI.

α4β2 nAChR (Fig. 3*A*), with scores equal to or below the threshold score derived from the benchmarking analysis (−637 Rosetta energy units) that separates bioactive from inactive α-GID mutants (*SI Appendix*, Fig. S3). As it was only feasible to experimentally test a subset of the α-GID bioactive predictions, we applied a series of evolutionary and sequence-based filters to identify positions on α-GID that were nonconserved, hydrophobic, and buried (Fig. 3*A* and *SI Appendix*, Fig. S4). These filters identified which of the 19 residues of α-GID might be open to point mutations that would not negatively affect function. Previous studies have demonstrated that making point mutations at positions that are nonconserved, hydrophobic, and buried can increase the odds of successful protein design (42–44).

First, to identify the nonconserved α-GID residues, a multiple sequence alignment of 20 α-conotoxins with the same spacing of cysteine residues (4/7) as α-GID was performed. Due to their role in conferring structural stability and function, the cysteine residues at positions 5, 6, 11, and 19 were completely conserved. Serine 7 and Proline 9, which comprise the well-known S-X-P motif (3), also had 95% and 90% sequence identity, respectively (Fig. 3*A* and *SI Appendix*, Fig. S4*A*). The remaining 13 positions, which all had sequence identity of less than or equal to 75%, were considered nonconserved (*SI Appendix*, Fig. S4*A*; marked with yellow stars in Fig. 3*A*). Second, using Chimera (45), the Kyte–Doolittle hydrophilicity was calculated for each position on α-GID, resulting in eight positions being identified as hydrophobic (hydropathy score > 0) (*SI Appendix*, Fig. S4*B*; marked with yellow stars in Fig. 3*A*). Third, Chimera was also used to calculate the solvent-accessible surface area (SASA) for each residue on α-GID in the ToxDock refined model. Three α-GID positions were clearly solvent-exposed, while the remaining 16 had a per-residue SASA of less than 150 Å^2 and were classified as buried (*SI Appendix*, Fig. S4*C*; marked with yellow stars in Fig. 3*A*). Two positions that met all three criteria of being nonconserved, hydrophobic, and buried were Ala-10 and Val-13 (Fig. 3*A* and *SI Appendix*, Fig. S4). Finally, phylogenetic analysis by maximum likelihood was performed on a set of 46 α-conotoxins from 24 different cone snail species. We found that position 13 is undergoing positive selection (*SI Appendix*, Table S2). Based on the three postdocking filters, we chose positions 10 (A10) and 13 (V13) of α-GID for making point mutations.

Specifically, two α-GID analogs with point mutations at position 10 (A10V and A10Q) and two analogs with point mutations at position 13 (V13I and V13Y) were chosen for synthesis and experimental assays. One of the peptides, α-GID[A10Q], had a score above threshold and was predicted to be inactive (Fig. 3*A*). Three of these peptides, α-GID[A10V], α-GID[V13I], and α-GID[V13Y], had scores below threshold and were predicted to be bioactive at the human α4β2 nAChR (Fig. 3*A*). These three predicted bioactives were chosen to select one relatively modest mutation (α-GID[V13I]) and two "riskier" mutations (α-GID[A10V] and α-GID[V13I]) that might also have novel function. For example, the prediction that the V13Y mutation would be bioactive (Fig. 3*A*) was surprising, as previous reports had speculated that aromatic residues could not be accommodated at that position due to the tight fit between the conotoxin and receptor (9, 18). However, inspection of the 25 lowest energy models that comprise the ToxDock ensemble showed that the hydroxyl group on the tyrosine's aromatic ring is capable of participating in buried polar interactions with backbone atoms on the receptor that could make this interaction favorable (Fig. 3*B*). Notably, all 25 models that comprise the ToxDock ensemble made polar contacts with the backbone of β2[L121]. In addition, depending on

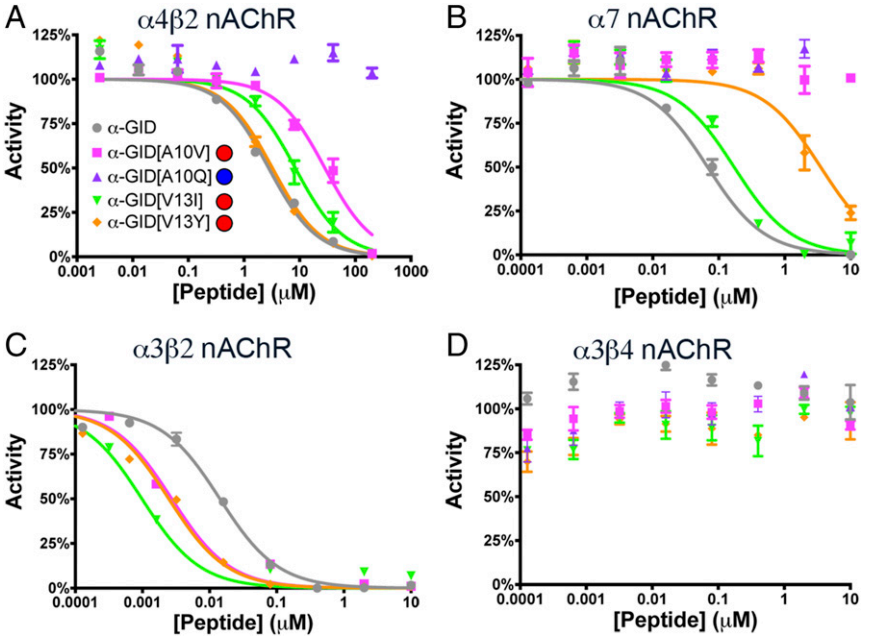

Fig. 4. Fluorescent membrane potential experiments. Inhibition of the human α4β2 (*A*), α7 (*B*), α3β2 (*C*), and α3β4 (*D*) nAChRs as a function of peptide concentration for native α-GID and the four peptides designed by ToxDock is shown. The peptides predicted to be bioactive at the α4β2 nAChR have red circles by their names, and the peptide predicted to be inactive has a blue circle. All dose–response experiments were performed using fluorescent membrane potential assays on HEK cell lines stably transfected with the respective combination of nAChR subunits. ACh concentrations used to evoke the currents were 30 μM for the α7 nAChR, 0.5 μM for the α4β2 nAChR, 1 μM for the α3β2 nAChR, and 5 μM for the α3β4 nAChR.

which conformer was considered, additional polar contacts were possible (Fig. 3*C*). Finally, the tyrosine aromatic ring appeared to pack tightly against β2[V111] and β2[F119] (Fig. 3*B*).

Experimental Characterization of α-GID Derivatives Identified with ToxDock at nAChRs. The four peptides identified by ToxDock (α-GID[A10V], α-GID[A10Q], α-GID[V13I], and α-GID[V13Y]) were synthesized, purified, and oxidatively folded as described previously (46) (*SI Appendix*, Fig. S5 *A* and *B* and Table S3). NMR structures of α-GID[A10V] (*SI Appendix*, Fig. S5*C*) and α-GID[V13Y] (*SI Appendix*, Fig. S5*D*) were solved (*SI Appendix*, Table S4) and indicated that both peptides adopted the expected conformations, with correct bonding of Cys-5 to Cys-11 and Cys-6 to Cys-19. The disulfide bond connectivities were determined based on the NMR data alone and were consistent with those found in wild-type α-GID.

Each α-GID derivative peptide was characterized experimentally with a fluorescent membrane potential assay to assess its ability to block the response to ACh of human α4β2, α7, α3β2, and α3β4 nAChRs in stably transfected HEK cells (14) (Fig. 4 and Table 1). All three peptides predicted to be bioactive by ToxDock (α-GID[A10V], α-GID[V13I], and α-GID[V13Y]) at the human α4β2 nAChR exhibited significant inhibition of this receptor (Fig. 4*A*). α-GID[V13Y] was the most potent analog, with an IC_{50} indistinguishable from the native peptide (IC_{50} = 3 μM), followed by α-GID[V13I] and α-GID[A10V] (IC_{50} = 8 μM and IC_{50} = 30 μM, respectively) (Fig. 4*A* and Table 1). Although α-GID[A10V] had the weakest antagonism overall, it was still bioactive at the human α4β2 nAChR. The peptide predicted by ToxDock to be inactive at the human α4β2 nAChR, α-GID[A10Q], displayed no antagonism of the receptor when tested at up to 200 μM (Fig. 4*A*). The ToxDock predictions were also confirmed when the peptides were tested with two-electrode voltage clamp electrophysiology (TEVC) at the rat α4β2 nAChR expressed in *Xenopus* oocytes (*SI Appendix*, Fig. S6*A*). Specifically, α-GID[A10V], α-GID[V13I], and α-GID[V13Y] were all bioactive at the rat α4β2 nAChR, while α-GID[A10Q] was inactive (*SI Appendix*, Fig. S6*A*). The TEVC results were reassuring, given that the rat and human α4β2 nAChR receptor binding pockets are nearly identical (*SI Appendix*, Fig. S6*B*).

The inhibitory activity of the α-GID derivative peptides was also examined at the human α3β2, α3β4, and α7 nAChRs (Fig. 4 *B–D* and Table 1). Perhaps due to the high conservation between the binding pockets of the α3β2 and α4β2 nAChRs, which differ by only a single methyl between the α3 and α4 subunits in the vicinity of these mutations (9) (*SI Appendix*, Fig. S7), all of the peptides bioactive at the α4β2 nAChR were also potent antagonists of the α3β2 nAChR (IC_{50} = 0.003 μM, IC_{50} = 0.001 μM, and IC_{50} = 0.002 μM for α-GID[A10V], α-GID[V13I], and α-GID[V13Y], respectively) (Fig. 4*C*). In addition, just as is the case with the native α-GID, none of the peptides displayed any antagonism at the α3β4 nAChR subtype (Fig. 4*D* and Table 1). Conotoxin α-AUIB was used as a positive control for the α3β4 nAChR and displayed the expected antagonism (IC_{50} = 0.1 μM; *SI Appendix*, Fig. S8).

While native α-GID is a strong antagonist of the human α7 nAChR (IC_{50} = 0.1 μM; Table 1), two of the peptides designed with ToxDock, α-GID[A10V] and α-GID[V13Y], had strongly diminished activity at the human α7 nAChR up to 10 μM (Fig. 4*B*). α-GID[A10V] had no discernable inhibition at up to 10 μM, although additional testing at 50 μM revealed

Table 1. Summary of experimental findings at human nAChRs

	α4β2 nAChR		IC_{50} at additional nAChRs, μM		
Peptide	ToxDock prediction	IC_{50}, μM	α7	α3β2	α3β4
α-GID		3	0.1	0.01	>10
α-GID[A10V]	Bioactive	30	>10	0.003	>10
α-GID[A10Q]	Inactive	>200	>10	>10	>10
α-GID[V13I]	Bioactive	8	0.2	0.001	>10
α-GID[V13Y]	Bioactive	3	4	0.002	>10

significant (73%), but not complete, inhibition of the human α7 nAChR at that concentration (*SI Appendix*, Fig. S9). It was also found that α-GID[V13Y] had reduced antagonism at the α7 nAChR, relative to the native, with an IC_{50} of 4 μM (Fig. 4*B* and Table 1). Taken together, these data indicate that α-GID[V13Y] and especially α-GID[A10V] discriminate against the human α7 nAChR.

Docking α-GID to the α4β2 nAChR Crystal Structure. As this paper was being prepared, the crystal structure of the α4β2 nAChR in complex with the agonist nicotine became available (31). We examined if our pose for α-GID in the homology model matched when docking it to this crystal structure (Fig. 5). Initially, there was a clash between loop C of the α4 subunit and α-GID after the conotoxin was superimposed onto the receptor. This clash was cleared by the Rosetta Relax phase of ToxDock (*SI Appendix*, Fig. S10). In the final pose after docking, the peptides in the crystal structure and homology model had a 1-Å Cα rmsd when aligned to each other. The largest differences in the poses were in the N- and C-terminal regions, which are the most flexible parts of the conotoxin (*SI Appendix*, Fig. S11). Key aromatic residues in the α4β2 nAChR binding pocket (47) had the same positions and rotamers in the two models (Fig. 5). On the α4 subunit, TyrC1, TyrC2, and TrpB all occupied the same positions and rotamers in the two models, and TrpD on the β2 subunit was in nearly the same position (Fig. 5). There were some differences, such as in the side-chain orientation of R12 on α-GID. Nonetheless, these data suggested that α-GID adopted largely the same docked poses in the crystal structure and homology model.

ToxDock Applied to Other Toxin Peptide:Ion Channel Systems. The generality of ToxDock was examined by measuring its redocking performance on three proteins of varying size and structure that bind peptide toxins and for which crystal structures have been determined. These were α-PnIA[A10L,D14K] and AChBP (α-PnIA:AChBP), Psalmotoxin and human acid-sensing ion channel (PcTx1:ASIC1a), and Charybdotoxin and a potassium channel ($CTX:K^+$) (36, 48, 49) (Fig. 6 *A*–*C* and *SI Appendix*, Figs. S12 and S13 *A*–*C*). In the redocking experiments, the peptide toxin was moved from its crystallographic pose using rotations and translations (*SI Appendix*, Fig. S12), and ToxDock was then applied to the perturbed pose to see if it could recover the native crystallographic orientation. In all three cases, at least one model in the ToxDock ensemble had a peptide Cα rmsd of less than 2.6 Å and within a factor of 2 of the lowest overall peptide Cα rmsd, indicating that the ensemble could capture near-native poses (*SI Appendix*, Fig. S13 *D* and *E*). Specifically, for the 16-residue α-PnIA[A10L,D14K], the lowest peptide Cα rmsd was 0.6 Å (Fig. 6*A*) and the mean over the ToxDock ensemble was 1.6 ± 0.5 Å (*SI Appendix*, Fig. S13 *A* and *E*). For Psalmotoxin, which is more than twice the size, with 40 amino acids, the lowest peptide Cα rmsd was 1.2 Å (Fig. 6*B*) and the mean peptide Cα rmsd over the ToxDock ensemble was 2.3 ± 0.4 Å (*SI Appendix*, Fig. S13 *B* and *E*). Charybdotoxin was the most challenging case overall, with a mean peptide Cα rmsd over the ToxDock ensemble of 5.7 ± 2.0 Å (*SI Appendix*, Fig. S13 *C* and *E*), but near-native poses were also captured as well; the lowest overall peptide Cα rmsd was 1.3 Å (Fig. 6*C*) and the lowest peptide Cα rmsd in the ensemble was 2.6 Å. Taken together, these data indicate that ToxDock is capable of modeling how medium to large peptide toxins dock to diverse ion channels.

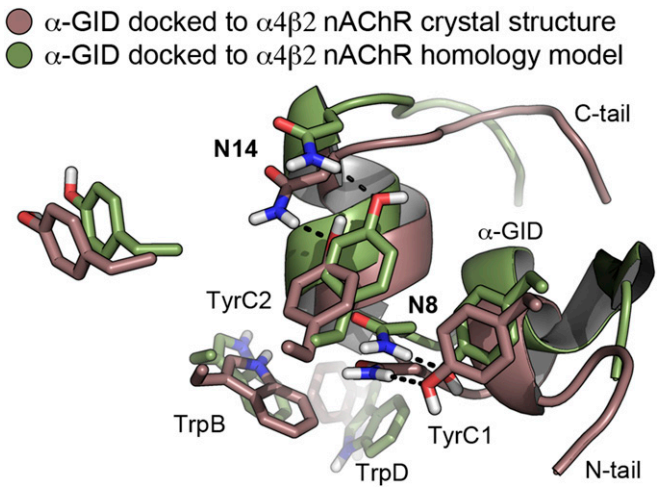

Fig. 5. Docking to α4β2 nAChR crystal structure in the desensitized state. The lowest energy poses of α-GID docked into the α4β2 nAChR homology model based on AChBP (green) and agonist-bound crystal structure (brown) with ToxDock are shown. Key aromatic residues on the nAChR are shown as sticks and labeled (TrpB, TyrC1, TyrC2, and TrpD). Residues on α-GID that participate in putative polar interactions (black dashed lines) are shown in sticks and labeled with bold text (N8 and N14). The receptor's backbone is omitted for clarity.

Discussion

Peptide toxins isolated from venomous creatures have played a major role in elucidating the structure and function of ion channels (1). In addition to nAChRs (50), venom peptides are used to study the structure and function of sodium (51), potassium (49), calcium (52), ASIC (48), and transient receptor potential (TRP) channels (53). Given the utility of animal venom peptides as probe compounds, their estimated abundance in the millions, and the challenge of synthesizing and screening them (46), new computational methods are needed to accelerate their discovery and development. Next-generation sequencing and proteomic discovery strategies would also benefit from computational approaches that help to narrow down which of the large number of putative toxins they identify are potentially active or selective for a given target (54). Structure-based virtual screening could be particularly useful in these contexts, but its potential has remained unclear due to the size of peptide toxins and the lack of crystal structures of the ion channels that they target. We addressed this challenge in the context of a homology model of the α4β2 nAChR, a prototypical ligand-gated ion channel, and the conotoxin α-GID that antagonizes it. Our two broad goals were to see if an algorithm for correctly docking α-GID and its analogs to the α4β2 nAChR could be developed by accounting for the conformational flexibility of these complexes, and if so, whether it could be used to discover new α-GID derivatives and those with functionally interesting properties.

One of our main findings is that, with extensive treatment of its conformational flexibility, a homology model of nAChR with less than 30% sequence identity to its template can be refined so that it is capable of discriminating between inactive and bioactive mutants of a conotoxin (Figs. 1 and 2). Using functional assays, we found that all four predictions from a virtual screen based on the homology model (Fig. 3) were correct (Fig. 4 and Table 1). The ability to identify bioactive α-GID mutants is particularly useful because the majority of mutants of α-GID that have been synthesized and tested are inactive. Two of the α-GID point mutants identified in the virtual screen, α-GID[A10V] and α-GID[V13Y], have substantially reduced antagonism at the human α7 nAChR. Using ToxDock, we showed that docking α-GID into two ostensibly dissimilar structures, the α4β2 nAChR crystallized with an agonist and an α4β2 nAChR homology model based on the AChBP/conotoxin template structure, resulted in similar poses for the peptide (Fig. 5). Finally, we confirmed the broader applicability of our docking program on

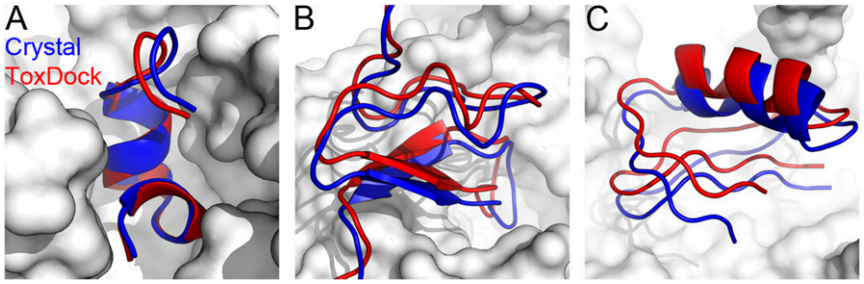

Fig. 6. Redocking experiments on diverse crystal structures. The crystallographic (blue) and lowest scoring redocked (red) pose of the toxin peptide in the ToxDock ensemble are shown for α-PnIA[A10L,D14K] bound to AChBP (*A*), Psalmotoxin bound to ASIC1a (*B*), and Charybdotoxin bound to a potassium channel (*C*). The surfaces of the binding protein and ion channels are shown in white. Renderings were made in PyMOL.

crystal structures of peptide toxins in complex with ion channels and a binding protein (Fig. 6). These findings are discussed in more detail below, along with possible future directions and improvements to the ToxDock method.

Importance of Conformational Sampling in Modeling the α-GID:α4β2 nAChR Complex. Our benchmarking experiments demonstrated that as more conformational sampling was included in the docking procedure, the ability of the refined homology model to discern between bioactive and inactive α-GID analogs improved (Fig. 2*A*). The identification of α-GID[V13Y] in the virtual screen also highlights how this extensive sampling is critical for making new predictions borne out by experiment. In the case of α-GID[V13Y], if the score for its interaction with the α4β2 nAChR had only used models based on a single conformation of the complex, then the favorable nature of its binding would have been underestimated. This is because different conformations of the channel and peptide captured different interactions, but no single conformation comprised all three interactions that were possible between the tyrosine hydroxyl group and the backbone amide and carbonyl groups of the receptor (Fig. 3*C*). Specifically, models based on conformation 2 captured that the hydroxyl group can form polar contacts with the amide group of β2[L121] and the carbonyl group of β2[N109], but did not predict any interactions with the carbonyl group of β2 [L121]. Conversely, models based on conformation 4 had polar contacts with the amide and carbonyl of β2[L121], but not with β2 [N109]. Thus, modeling α-GID[V13Y] as a superposition of these different conformers allowed the favorable nature of its interactions with the α4β2 nAChR to be captured more fully than if only a single conformation had been used and led to the correct prediction that it would be bioactive. Experimental validation of this prediction was particularly gratifying, given that the nearly identical α-GID[V13F] has been shown to be inactive at the rat α4β2 nAChR (9).

Extensive computational sampling also played a role when docking α-GID to the agonist-bound crystal structure of the α4β2 nAChR (Fig. 5). It was unclear if docking α-GID to the α4β2 nAChR agonist-bound structure could lead to agreement with the homology model because the nAChR binding pocket undergoes significant rearrangement depending on whether an agonist or antagonist is present (25, 33, 34). We found that the poses of α-GID in the α4β2 nAChR crystal structure or AChBP-derived homology model were similar after refinement with ToxDock, and that initial steric collisions between the conotoxin and loop C were alleviated through global relaxation of the receptor backbone. The concordance between the poses of α-GID in the two models suggests they have captured the binding pose of α-GID reasonably well. More broadly, our finding raises the possibility that the extracellular domains of agonist-bound nAChR structures could potentially be used as an alternative to, or in conjunction with, AChBP-derived homology models for docking conotoxins, provided they are subject to appropriate refinement.

α-GID Analogs with Useful Properties. A key finding from this study is that two of the three α-GID analogs identified by the virtual screen, α-GID[A10V] and α-GID[V13Y], had the long-sought-after property of reduced activity at the human α7 nAChR without sacrificing their activity at the α4β2 nAChR. These findings suggest that even a relatively modest virtual screen of 256 α-GID point mutants, further focused by the use of post-docking filters, can uncover novel peptide ligands with favorable properties. This result agrees with the recent α-GID modeling study of Suresh and Hung (15). Using sophisticated umbrella sampling and free-energy calculations, they came to the conclusion that a point mutation on the N-terminal tail, a different region of α-GID than the one we focused on, could potentially also impart specificity for the α4β2 nAChR (15). More generally, our findings are in accord with published results of Hogg et al. (55) and Luo et al. (56), who showed that a single-residue alteration in a similar conotoxin, α-PnIA, is sufficient for switching its nAChR subtype selectivity.

A mechanistic hypothesis for why α-GID[V13Y] has reduced activity at the human α7 nAChR can be developed by comparing the binding pockets of the α4β2 and α7 nAChRs. In the case of α-GID[V13Y], the lack of a T-shaped pi-stack with β2[F119] (which is a glutamine in the α7 nAChR) and the additional steric hindrance from a leucine in the α7 nAChR (which is Val-111 in the α4β2 nAChR) positioned close to the tyrosine side chain may have sufficed to cause the loss of activity at the α7 nAChR. In a broad sense, chemical novelty conferred new biological properties, which is often the case for docking and virtual screening studies of small molecules (57). Mutations at other positions may also result in α-GID derivatives that discriminate against the α7 nAChR. For example, the hydrophobic, conservation, and buried residue filters used to pinpoint positions 10 and 13 for making mutations were also in agreement that position 18 would be a viable choice for making mutations. Since this is the position at which the α-GID mutant selective for the rat α4β2 nAChR vs. the α3β2 nAChR was discovered, it implies that integrating additional sources of information such as evolutionary data can help to accelerate the discovery of optimized mutations by pinpointing the most promising sites to search for mutations (54, 58).

Combining the mutations identified in this study with those previously found (9–11) may facilitate the development of an α-GID derivative that is truly selective for the α4β2 nAChR. However, to be effective as a tool compound, the potency of such an α-GID analog at the α4β2 nAChR would also need to be increased into the low nanomolar range, commensurate with other classical conotoxin probes such as MII (4). One particularly promising route for achieving this aim could be developing α-GID analogs with noncanonical amino acids (NCAAs), which

Hopping et al. (18) used to increase the potency of the conotoxin α-PnIA at the α7 nAChR. The recent incorporation of NCAAs into Rosetta could also facilitate such an effort (59). Finally, the design of more potent α-GID analogs could exploit our finding that α-GID[V13Y] is ∼1,000-fold weaker at the α4β2 nAChR than at the α3β2 nAChR despite only one residue differing between the α3 and α4 subunits in the vicinity of α-GID[Y13]. Since this residue is a threonine on the α4 subunit and a serine on the α3 subunit, it appears that the presence of a single additional methyl group in α4 may account for the much weaker potency of α-GID[V13Y] at the α4β2 nAChR. Thus, a design consideration when choosing canonical or noncanonical mutations to α-GID appears to be avoiding steric clashes with α4[Thr157].

As specialized methods for peptide toxin synthesis and nAChR screening continue to be developed, such as parallelized oxidative folding (60) and high-throughput electrophysiology (61), it may become possible to test the majority of bioactive predictions made by a virtual screen with ToxDock to discover additional analogs with novel activity.

Improvements to ToxDock. Two improvements to ToxDock could be made that would enhance its generality and utility. First, both computational and experimental efforts have demonstrated that the interaction of peptide toxins with the cellular membrane can play a key role in their docking to ion channels (62–64). Thus, the addition of an explicit or implicit representation of the membrane to ToxDock might help it to model peptide toxin:ion channel docking for systems like TRP and sodium channels where membrane interactions are important. Second, combining ToxDock with a protocol for estimating relative binding affinities would enable ToxDock to go beyond prediction of bioactivity to guide improvements in potency of peptide toxin analogs. Since one of the most important components of an affinity calculation is a realistic binding pose, which ToxDock appears to achieve reasonably well for both homology models and crystal structures, it is possible that using ToxDock-derived poses as the basis for free-energy perturbation (FEP) calculations could yield estimates of relative binding affinities for peptide toxin mutants. Recent efforts suggest that computing relative binding affinities for peptide toxin and channel systems is within the domain of applicability of FEP (65). However, given that FEP calculations are sensitive to the amount of conformational reorganization that a protein undergoes (66, 67), it is possible that specialized enhanced sampling protocols may need to be developed to fully accommodate the flexibility of conotoxins like α-GID.

In summary, this study demonstrates the feasibility of a combined computational and experimental approach for an α-conotoxin and nAChR and opens up the possibility of it being applied to the growing number of identified peptide toxins and their ion channel targets. Moreover, it highlights the value in using extensive conformational sampling to model peptide toxin:ion channel complexes and what kind of functional and structural data are necessary for validating those efforts. To facilitate such studies, we have made ToxDock publicly available as a server that can be freely and easily used by any member of the academic research community (rosie.rosettacommons.org/tox_dock).

Materials and Methods

Homology Modeling. The α4β2 nAChR extracellular domain dimer was modeled using Modeller (68) version 9.11 based on the X-ray structures of AChBP from *A. californica* in complex with the peptide toxins α-PnIA [A10L, D14K], α-ImI, α-BuIA, and α-TxIA[A10L] [Protein Data Bank (PDB) ID codes 2BR8, 2C9T, 2BYP, 4EZ1, and 2UZ6, respectively] (33, 36–38). The alignment between AChBP and the nAChR sequences was based on a multiple sequence alignment presented previously (47). The sequence identity between AChBP and the extracellular domains was 27.8% and 23.4% for the α4 and β2 subunits, respectively.

Docking and Virtual Screening. Docking and virtual screening of α-GID and α-GID analogs against the α4β2 nAChR homology model was performed using our ensemble-docking algorithm, ToxDock, using Rosetta revision 57232 and the talaris2013 weight set. ToxDock is available at rosie.rosettacommons.org/tox_dock. Models of α-GID mutants were based on its NMR structure (PDB ID code 1MTQ) (11). Apo rotamers for AChBP were obtained from PDB ID code 2Y7Y (69).

Molecular Dynamics Simulation. Molecular dynamics simulations were completed using DESMOND version 4.4 (70) with the OPLS3 forcefield after preparation with the System Builder workflow (Schrödinger).

Peptide Synthesis. All peptides were synthesized by The Rockefeller University Proteomics Center using Fmoc solid-phase peptide synthesis as previously described (46).

NMR Solution Structure Derivation. Standard homonuclear NMR techniques were used to solve the solution structures of α-GID[A10V] and α-GID[V13Y]. Data were collected at 7 °C, and structures were obtained via simulated annealing and explicit water refinement, using nuclear Overhauser effect (NOE) distance restraints and chemical shift-derived angular restraints as input for the calculations. The temperature of 7 °C was chosen to maximize the number and intensity of observable NOE distance restraints and also for consistency with previous NMR studies of α-GID (11). For final calculations, hydrogen and disulfide bonds consistent with the NMR data and preliminary structures were also included in the calculations.

Fluorescent Membrane Potential Assay. For functional tests of nAChRs expressed in HEK cells, we used a FLEXstation (Molecular Devices) bench-top scanning fluorimeter as described by Kuryatov et al. (14). To increase the expression level of α3β2 nAChRs, the plates were incubated at 29 °C for 20 h before being tested. The α7 cell line was tested as described by Kuryatov et al. (71). A membrane potential fluorescent indicator kit (Molecular Devices) was used according to the manufacturer's protocols. Peptides were added 1 h before recordings. ACh concentrations used to evoke currents were 30 μM for the α7 nAChR, 0.5 μM for the α4β2 nAChR, 1 μM for the α3β2 nAChR, and 5 μM for the α3β4 nAChR. All recordings were performed at 29 °C. Each data point was averaged from three responses from separate wells. IC_{50} values were calculated from a nonlinear fit of the Hill equation to the data (GraphPad Prism version 7.0). Native α-GID was purchased from Smartox Biotechnology. Conotoxins AuIB and MII were purchased from Tocris.

Electrophysiological Measurements. The nAChR cDNAs were provided by J. Patrick, Baylor College of Medicine, Houston, TX, and subcloned into the oocyte expression vector pNKS2. The cRNA was synthesized with the SP6 mMessage mMachine kit (Ambion), and *Xenopus laevis* (Nasco International) oocytes were injected with 50-nL aliquots of cRNA (0.05 mg/mL). The nAChR subunits were mixed at the ratio of 5:1 (α4:β2).

Antagonist dose–response curves were measured as described (72) in ND96 (96 mM NaCl, 2 mM KCl, 1 mM $CaCl_2$, 1 mM $MgCl_2$, and 5 mM Hepes at pH 7.4). Briefly, current responses to 100 μM Ach were recorded at −70 mV using a Turbo Tec 05X Amplifier (NPI Electronic) and Cell Works software. A fast and reproducible solution exchange (<300 ms) was achieved with a 50-μL funnel-shaped oocyte chamber combined with a fast solution flow (∼150 $\mu L \cdot s^{-1}$) fed through a custom-made manifold mounted immediately above the oocyte. Agonist pulses were applied for 2 s at 4-min intervals. Peptides were applied for 3 min in a static bath. IC_{50} values were calculated from a nonlinear fit of the Hill equation to the data (GraphPad Prism version 6.0). Data are presented as mean ± SE from at least three experiments.

ACKNOWLEDGMENTS. Expert technical assistance from Stephen Leak, Shenglong Wang, and Stratos Efstathiadis at the New York University High-Performance Computing facility and help from Jianqin Zhuang in setting up and optimizing the NMR experiments are sincerely appreciated. A.E.L. acknowledges support from NIH Training Grant T32MH096331-04S1; a travel grant from the Sackler Institute of Graduate Biomedical Sciences; and illuminating conversations with David Borhani, Evan Baugh, Anthony Nicholls, John Karanicolas, Avner Schlessinger, Richard De Veaux, and Timothy Jacobs. B.R. acknowledges funding from NIH Grants R01-NS030989 and P01-NS074972. R.B. acknowledges funding from New York University, the NIH, and the Simons Foundation. M.H. acknowledges funding from the Camille and Henry Dreyfus Teacher-Scholar Award and National Science Foundation (NSF) Awards CHE-1247550 and CHE-1228921. J.G. acknowledges

funding from the City University of New York Graduate Center. S.L. was supported by NIH Grant R01-GM073151. A.N. was supported by the Deutsche Forschungsgemeinschaft (NI 592/7-1). S.F.P. acknowledges support from NSF Grant MCB-1253277.

1. Kalia J, et al. (2015) From foe to friend: Using animal toxins to investigate ion channel function. *J Mol Biol* 427:158–175.
2. King GF (2015) *Venoms to Drugs: Venom as a Source for the Development of Human Therapeutics* (Royal Society of Chemistry, Cambridge).
3. Lewis RJ, Dutertre S, Vetter I, Christie MJ (2012) Conus venom peptide pharmacology. *Pharmacol Rev* 64:259–298.
4. McIntosh JM, Santos AD, Olivera BM (1999) Conus peptides targeted to specific nicotinic acetylcholine receptor subtypes. *Annu Rev Biochem* 68:59–88.
5. Jackson KJ, Sanjakdar SS, Muldoon PP, McIntosh JM, Damaj MI (2013) The α3β4* nicotinic acetylcholine receptor subtype mediates nicotine reward and physical nicotine withdrawal signs independently of the α5 subunit in the mouse. *Neuropharmacology* 70:228–235.
6. Napier IA, et al. (2012) Intrathecal α-conotoxins Vc1.1, AuIB and MII acting on distinct nicotinic receptor subtypes reverse signs of neuropathic pain. *Neuropharmacology* 62: 2202–2207.
7. Olivera BM, Quik M, Vincler M, McIntosh JM (2008) Subtype-selective conopeptides targeted to nicotinic receptors: Concerted discovery and biomedical applications. *Channels (Austin)* 2:143–152.
8. Romero HK, et al. (2017) Inhibition of alpha9alpha10 nicotinic acetylcholine receptors prevents chemotherapy-induced neuropathic pain. *Proc Natl Acad Sci USA* 114: E1825–E1832.
9. Banerjee J, et al. (2014) Design and synthesis of α-conotoxin GID analogues as selective α4β2 nicotinic acetylcholine receptor antagonists. *Biopolymers* 102:78–87.
10. Millard EL, et al. (2009) Inhibition of neuronal nicotinic acetylcholine receptor subtypes by alpha-Conotoxin GID and analogues. *J Biol Chem* 284:4944–4951.
11. Nicke A, et al. (2003) Isolation, structure, and activity of GID, a novel alpha 4/7-conotoxin with an extended N-terminal sequence. *J Biol Chem* 278:3137–3144.
12. Muñoz W, Rudy B (2014) Spatiotemporal specificity in cholinergic control of neocortical function. *Curr Opin Neurobiol* 26:149–160.
13. Taly A, Corringer PJ, Guedin D, Lestage P, Changeux JP (2009) Nicotinic receptors: Allosteric transitions and therapeutic targets in the nervous system. *Nat Rev Drug Discov* 8:733–750.
14. Kuryatov A, Luo J, Cooper J, Lindstrom J (2005) Nicotine acts as a pharmacological chaperone to up-regulate human alpha4beta2 acetylcholine receptors. *Mol Pharmacol* 68:1839–1851.
15. Suresh A, Hung A (2016) Molecular simulation study of the unbinding of α-conotoxin [γ4E]GID at the α7 and α4β2 neuronal nicotinic acetylcholine receptors. *J Mol Graph Model* 70:109–121.
16. Dani JA, Bertrand D (2007) Nicotinic acetylcholine receptors and nicotinic cholinergic mechanisms of the central nervous system. *Annu Rev Pharmacol Toxicol* 47:699–729.
17. Dutertre S, Lewis RJ (2004) Computational approaches to understand alpha-conotoxin interactions at neuronal nicotinic receptors. *Eur J Biochem* 271:2327–2334.
18. Hopping G, et al. (2014) Hydrophobic residues at position 10 of α-conotoxin PnIA influence subtype selectivity between α7 and α3β2 neuronal nicotinic acetylcholine receptors. *Biochem Pharmacol* 91:534–542.
19. Jin AH, et al. (2008) Molecular engineering of conotoxins: The importance of loop size to alpha-conotoxin structure and function. *J Med Chem* 51:5575–5584.
20. Luo S, et al. (2010) Atypical alpha-conotoxin LtIA from Conus litteratus targets a novel microsite of the alpha3beta2 nicotinic receptor. *J Biol Chem* 285:12355–12366.
21. Talley TT, et al. (2006) Alpha-conotoxin OmIA is a potent ligand for the acetylcholine-binding protein as well as alpha3beta2 and alpha7 nicotinic acetylcholine receptors. *J Biol Chem* 281:24678–24686.
22. Kasheverov IE, et al. (2016) High-affinity α-conotoxin PnIA analogs designed on the basis of the protein surface topography method. *Sci Rep* 6:36848.
23. King MD, Long T, Andersen T, McDougal OM (2016) Genetic algorithm managed peptide mutant screening: Optimizing peptide ligands for targeted receptor binding. *J Chem Inf Model* 56:2378–2387.
24. Doupnik CA, Parra KC, Guida WC (2014) A computational design approach for virtual screening of peptide interactions across K(+) channel families. *Comput Struct Biotechnol J* 13:85–94.
25. Rucktooa P, Smit AB, Sixma TK (2009) Insight in nAChR subtype selectivity from AChBP crystal structures. *Biochem Pharmacol* 78:777–787.
26. Carlsson J, et al. (2011) Ligand discovery from a dopamine D3 receptor homology model and crystal structure. *Nat Chem Biol* 7:769–778.
27. McGovern SL, Shoichet BK (2003) Information decay in molecular docking screens against holo, apo, and modeled conformations of enzymes. *J Med Chem* 46:2895–2907.
28. Das R, Baker D (2008) Macromolecular modeling with rosetta. *Annu Rev Biochem* 77: 363–382.
29. Raveh B, London N, Schueler-Furman O (2010) Sub-angstrom modeling of complexes between flexible peptides and globular proteins. *Proteins* 78:2029–2040.
30. Tyka MD, et al. (2011) Alternate states of proteins revealed by detailed energy landscape mapping. *J Mol Biol* 405:607–618.
31. Morales-Perez CL, Noviello CM, Hibbs RE (2016) X-ray structure of the human α4β2 nicotinic receptor. *Nature* 538:411–415.
32. Azam L, et al. (2015) Molecular interaction of α-conotoxin RgIA with the rat α9α10 nicotinic acetylcholine receptor. *Mol Pharmacol* 87:855–864.
33. Hansen SB, et al. (2005) Structures of Aplysia AChBP complexes with nicotinic agonists and antagonists reveal distinctive binding interfaces and conformations. *EMBO J* 24: 3635–3646.
34. Hibbs RE, Radic Z, Taylor P, Johnson DA (2006) Influence of agonists and antagonists on the segmental motion of residues near the agonist binding pocket of the acetylcholine-binding protein. *J Biol Chem* 281:39708–39718.
35. Zouridakis M, et al. (2014) Crystal structures of free and antagonist-bound states of human α9 nicotinic receptor extracellular domain. *Nat Struct Mol Biol* 21: 976–980.
36. Celie PH, et al. (2005) Crystal structure of nicotinic acetylcholine receptor homolog AChBP in complex with an alpha-conotoxin PnIA variant. *Nat Struct Mol Biol* 12: 582–588.
37. Dutertre S, et al. (2007) AChBP-targeted alpha-conotoxin correlates distinct binding orientations with nAChR subtype selectivity. *EMBO J* 26:3858–3867.
38. Ulens C, et al. (2006) Structural determinants of selective alpha-conotoxin binding to a nicotinic acetylcholine receptor homolog AChBP. *Proc Natl Acad Sci USA* 103: 3615–3620.
39. London N, Gullá S, Keating AE, Schueler-Furman O (2012) In silico and in vitro elucidation of BH3 binding specificity toward Bcl-2. *Biochemistry* 51:5841–5850.
40. Muttenthaler M, Akondi KB, Alewood PF (2011) Structure-activity studies on alpha-conotoxins. *Curr Pharm Des* 17:4226–4241.
41. Baugh EH, Lyskov S, Weitzner BD, Gray JJ (2011) Real-time PyMOL visualization for Rosetta and PyRosetta. *PLoS One* 6:e21931.
42. Bulaj G, et al. (2001) Delta-conotoxin structure/function through a cladistic analysis. *Biochemistry* 40:13201–13208.
43. Karanicolas J, Kuhlman B (2009) Computational design of affinity and specificity at protein-protein interfaces. *Curr Opin Struct Biol* 19:458–463.
44. Stranges PB, Kuhlman B (2013) A comparison of successful and failed protein interface designs highlights the challenges of designing buried hydrogen bonds. *Protein Sci* 22:74–82.
45. Meng EC, Pettersen EF, Couch GS, Huang CC, Ferrin TE (2006) Tools for integrated sequence-structure analysis with UCSF Chimera. *BMC Bioinformatics* 7:339.
46. Anand P, et al. (2014) Sample limited characterization of a novel disulfide-rich venom peptide toxin from terebrid marine snail Terebra variegata. *PLoS One* 9:e94122.
47. Xiu X, Puskar NL, Shanata JA, Lester HA, Dougherty DA (2009) Nicotine binding to brain receptors requires a strong cation-pi interaction. *Nature* 458:534–537.
48. Baconguis I, Gouaux E (2012) Structural plasticity and dynamic selectivity of acid-sensing ion channel-spider toxin complexes. *Nature* 489:400–405.
49. Banerjee A, Lee A, Campbell E, Mackinnon R (2013) Structure of a pore-blocking toxin in complex with a eukaryotic voltage-dependent K(+) channel. *eLife* 2:e00594.
50. Changeux JP, Kasai M, Lee CY (1970) Use of a snake venom toxin to characterize the cholinergic receptor protein. *Proc Natl Acad Sci USA* 67:1241–1247.
51. Osteen JD, et al. (2016) Selective spider toxins reveal a role for the Nav1.1 channel in mechanical pain. *Nature* 534:494–499.
52. McCleskey EW, et al. (1987) Omega-conotoxin: Direct and persistent blockade of specific types of calcium channels in neurons but not muscle. *Proc Natl Acad Sci USA* 84:4327–4331.
53. Cao E, Liao M, Cheng Y, Julius D (2013) TRPV1 structures in distinct conformations reveal activation mechanisms. *Nature* 504:113–118.
54. Verdes A, et al. (2016) From mollusks to medicine: A venomics approach for the discovery and characterization of therapeutics from Terebridae peptide toxins. *Toxins (Basel)* 8:117.
55. Hogg RC, et al. (1999) Single amino acid substitutions in alpha-conotoxin PnIA shift selectivity for subtypes of the mammalian neuronal nicotinic acetylcholine receptor. *J Biol Chem* 274:36559–36564.
56. Luo S, et al. (1999) Single-residue alteration in alpha-conotoxin PnIA switches its nAChR subtype selectivity. *Biochemistry* 38:14542–14548.
57. Manglik A, et al. (2016) Structure-based discovery of opioid analgesics with reduced side effects. *Nature* 537:185–190.
58. Puillandre N, Holford M (2010) The Terebridae and teretoxins: Combining phylogeny and anatomy for concerted discovery of bioactive compounds. *BMC Chem Biol* 10:7.
59. Renfrew PD, Choi EJ, Bonneau R, Kuhlman B (2012) Incorporation of noncanonical amino acids into Rosetta and use in computational protein-peptide interface design. *PLoS One* 7:e32637.
60. Murray JK, et al. (2016) Single residue substitutions that confer voltage-gated sodium ion channel subtype selectivity in the NaV1.7 inhibitory peptide GpTx-1. *J Med Chem* 59:2704–2717.
61. Sidach SS, Fedorov NB, Lippiello PM, Bencherif M (2009) Development and optimization of a high-throughput electrophysiology assay for neuronal alpha4beta2 nicotinic receptors. *J Neurosci Methods* 182:17–24.
62. Bae C, et al. (2016) Structural insights into the mechanism of activation of the TRPV1 channel by a membrane-bound tarantula toxin. *eLife* 5:e11273.
63. Drane SB, et al. (2017) Structure and activity of contryphan-Vc2: Importance of the D-amino acid residue. *Toxicon* 129:113–122.
64. Wang J, et al. (2011) Mapping the receptor site for alpha-scorpion toxins on a Na+ channel voltage sensor. *Proc Natl Acad Sci USA* 108:15426–15431.
65. Kuyucak S, Norton RS (2014) Computational approaches for designing potent and selective analogs of peptide toxins as novel therapeutics. *Future Med Chem* 6: 1645–1658.
66. Clark AJ, et al. (2016) Free energy perturbation calculation of relative binding free energy between broadly neutralizing antibodies and the gp120 glycoprotein of HIV-1. *J Mol Biol* 429:930–947.

67. Lim NM, Wang L, Abel R, Mobley DL (2016) Sensitivity in binding free energies due to protein reorganization. *J Chem Theory Comput* 12:4620–4631.
68. Fiser A, Sali A (2003) Modeller: Generation and refinement of homology-based protein structure models. *Methods Enzymol* 374:461–491.
69. Ulens C, et al. (2009) Use of acetylcholine binding protein in the search for novel alpha7 nicotinic receptor ligands. In silico docking, pharmacological screening, and X-ray analysis. *J Med Chem* 52:2372–2383.
70. Bowers KJ, et al. (2006) Scalable algorithms for molecular dynamics simulations on commodity clusters. *ACM/IEEE Conference on Supercomputing (SC06)* (ACM Press, New York).
71. Kuryatov A, Mukherjee J, Lindstrom J (2013) Chemical chaperones exceed the chaperone effects of RIC-3 in promoting assembly of functional α7 AChRs. *PLoS One* 8:e62246.
72. Beissner M, et al. (2012) Efficient binding of 4/7 α-conotoxins to nicotinic α4β2 receptors is prevented by Arg185 and Pro195 in the α4 subunit. *Mol Pharmacol* 82:711–718.